THE JOURNAL OF PHYSICAL CHEMISTRY B

Article

pubs.acs.org/JPCB

Ordered Self-Similar Patterns in Anisotropic Stochastic Growth

Zhenwei Yao[†,⊥] and Monica Olvera de la Cruz*[,†,‡,§,∥]

[†]Department of Materials Science and Engineering, [‡]Department of Chemistry, [§]Department of Chemical and Biological Engineering, and [∥]Department of Physics, Northwestern University, Evanston, Illinois 60208-3108, United States

[⊥]Department of Physics and Astronomy, and Institute of Natural Sciences, Shanghai Jiao Tong University, Shanghai 200240, China

ABSTRACT: We propose an anisotropic stochastic growth model to rationalize the anisotropic self-assembly of supramolecules to form elongated two-dimensional ribbon structures in a recent experiment. The model exhibits distinct growth scenarios that are critically controlled by the ratio of the transverse and the longitudinal growth rate. In the regime of suppressed transverse growth, the model generates the experimentally observed elongated structures through layer-by-layer growing. We further observe the convergence of rough clusters toward smooth regular elliptic patterns by averaging over a number of independent growth processes. Remarkably, these resulting elliptic clusters are self-similar in each instantaneous moment in the growth process. Statistical analysis suggests that the realization of such ordered patterns does not rely on the delicate coordination of different parts in the cluster growth. The self-similarity phenomenon derived from this idealized model may have wider implications, notably in the designed clustering of various elementary building blocks with anisotropic interactions.

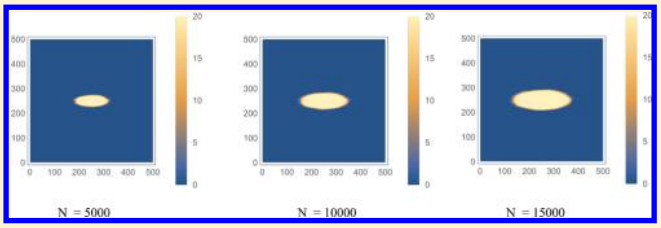

INTRODUCTION

Self-assembly phenomena are widely seen in natural and artificial systems, and they provide an efficient and reliable routine to synthesize materials with desired properties down to the nanometer scale.[1,2] Of special interest is the design of anisotropic self-assembly routines that can produce phases not found in isotropic growth processes. New technologies have been developed to introduce the elements of anisotropy through the design of anisotropic interactions[3−6] and the fabrication of anisotropic particles like Janus particles,[7] patchy particles,[4,8] branched particles,[9] and dimpled particles.[10] In supramolecular self-assembly, highly anisotropic molecular components represent the majority of building blocks, including peptide amphiphiles,[11] DNA-coated nanoparticles,[3] polymers,[12] lipid-DNA complexes,[13] and nanofibers.[14] Recently, perylene monoimide (PMI) based chromophore amphiphiles (CA) have been synthesized and observed to self-assemble into highly elongated ribbon structures whose length $L \sim$ several microns, width $w = 40 \pm 7$ nm and thickness $t = 2.3 \pm 0.4$ nm.[15] These self-assembled complexes of soft materials, inspired by the internal structure of chloroplasts in plants, integrate the necessary chemically functioning components and have many potential applications in complex devices, materials design, and renewable energy.[16] Using dynamic simulations to investigate the resulting ribbon structures from the CA molecules is a grand challenge given the large size of the system and the considerable computational resources required to simulate the structured molecular components whose anisotropic property is indispensable in accounting for the elongated structures.

The self-assembly of CA molecules into the highly coherent structures observed in the above-mentioned experiment inspired us to propose an idealized growth model to rationalize the anisotropic self-assembly process.[15] Among stochastic[17,18] and deterministic[19,20] growth models, the fluctuations in the convoluted aggregation of CA molecules justify a probability description. In comparison with the computationally demanding large scale dynamic simulations required to address the growth phenomena in far-from-equilibrium conditions, a stochastic model can provide valuable insights into the formation mechanism of featured patterns in a growth process by capturing the essential physics without diving into irrelevant finer details.

As one of the earliest models of stochastic growth, the Eden growth model[17] and its variations[18,21−23] have successfully described a variety of biological growth processes like the growth of bacterial colonies and tumor proliferation.[24] The Eden growth model is a lattice model where one particle is added at a time in randomly chosen sites adjacent to the occupied sites. To explore the highly elongated structures fabricated from the elementary CA molecules in the experiment it is necessary to generalize the original Eden growth model to account for the anisotropic force that pulls the molecules together in the form of the relatively stronger longitudinal $\pi-\pi$ stacking and the transverse edge−edge stacking.[15] The anisotropic case of the Eden growth model has been briefly discussed in ref 17 and 24 where snapshots of a growing elongated cluster have been shown but further detailed analysis has not been done to reveal the pattern in these configurations.

Special Issue: William M. Gelbart Festschrift

Received: February 22, 2016
Revised: March 21, 2016
Published: March 22, 2016

DOI: 10.1021/acs.jpcb.6b01789
J. Phys. Chem. B 2016, 120, 5960−5965

In this work, we study the anisotropic stochastic growth process in the frame of the generalized Eden growth model. The objective of this work is to understand the principle of self-organization in the fabrication of the ribbon structures out of the elementary CA molecules[15] and, more broadly, to seek the patterns hidden in the convoluted indeterministic growth processes not found in the preceding works.[17,24]

In our growth model, we introduce two probabilities p_l and p_t to characterize the differential in the growth rates along the longitudinal and the transverse directions, respectively. The model successfully produces highly elongated ribbon structures when the longitudinal growth dominates over the transverse growth. The entire growth process is a history dependent stochastic process. The occupation of a site in any previous step will influence the landing of a future particle onto the cluster. Simulations reveal that summation over a number of such highly indeterministic processes can ultimately lead to smooth elliptic clusters. Remarkably, we find the self-similarity in each instantaneous shape of an averaged growing cluster. The aspect ratio of the elliptic cluster in the entire growth process is an invariant for given p_l and p_t. We further show the statistical independence in the transverse growth underlying the self-similarity phenomenon, suggesting that the realization of the self-similar growth process does not require the coordinated growth of different parts in the cluster. This work may provide a new dimension to interpret the clustering of various elementary building blocks that interact with anisotropic interaction potentials and have implications in the design of both 2D and 3D aggregates for desired exterior shapes.

MODEL

It is experimentally characterized that the elementary CA molecules form a slightly distorted 2D rectangular crystalline lattice.[15] We therefore design a rectangular lattice as shown in Figure 1, where an occupied site represents a CA molecule. The

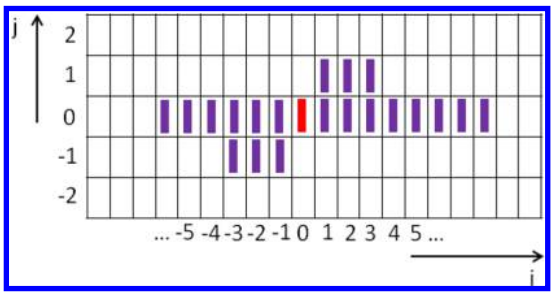

Figure 1. Schematic plot of the stochastic growth model. A cluster forms with the occupation of empty sites.

colored bars in Figure 1 represent the CA molecules that grow along both the longitudinal (the axis of i in Figure 1) and the transverse (the axis of j) directions. The aggregation process of CA molecules starts from the central red bar in Figure 1. One CA molecule is added in each step. So the total number of the occupied sites is equal to the frame number in this dynamic growth. To account for the chemical asymmetry of CA molecules, we introduce two probabilities: p_l and p_t, the probability of adding a new molecule in the longitudinal and transverse directions around an isolated occupied site in the lattice, respectively. These distinct probabilities characterize the effect of the anisotropic forces that pull the molecules together in the form of the longitudinal $\pi-\pi$ stacking and the transverse edge−edge stacking. Here, $p_l > p_t$, because the $\pi-\pi$ stacking is stronger than the edge−edge stacking. The charge screening by adding salt is expected to reduce this difference. Without loss of generality, we set $p_l = 1$. Therefore, the only parameter in the model to control the morphological evolution of the occupied area is p_t.

The rule to occupy a new site in the update of the configuration is first to calculate the probability of each available unoccupied site and then identify the specific site to be occupied. Specifically, the probability of occupying an available site i is

$$p_i = \sum_{\langle i,j \rangle} s_j \tag{1}$$

where the summation is over the four nearest neighbors around the site i. The state of an occupied site is $s_j = 1$; otherwise, $s_j = 0$. According to eq 1, an available site with both longitudinal and transverse neighbors (like the empty box below the red bar in Figure 1) has the probability of $p_l + p_t$ to be occupied in a new step. In simulations, vacancies may appear that are surrounded by four occupied sites. These vacancies have the highest probability to be filled in the update of the system. The rule of eq 1 prescribes that only the empty sites (labeled from $k = 1$ to m) adjacent to the occupied ones are assigned with a nonzero probability p_k ($k = 1, 2, 3...m$). In order to identify the specific site to be occupied, we first normalize the values for p_k by redefining

$$\tilde{p}_k = \frac{p_k}{\sum_{j=1}^{m} p_j} \tag{2}$$

where the summation is over all the possible sites adjacent to the occupied region. Then we pick up a random number r between zero and unity from a uniform distribution. According to the interval where the value of r falls, say $r \in (p_k, p_{k+1})$, we decide the site to be occupied is k.

In comparison with the diffusion-limit aggregation where a new particle is added to the cluster by random walk, the randomness of adding a new particle in our model is defined in terms of p_l and p_t.[18] Consequently, we obtain compact clusters as observed in experiment[15] instead of less compact fractal configurations.[18] The complexity in the seemingly simple rules by eqs 1 and 2 lies in the long-range temporal correlations in the construction of a growing cluster. The occupation of a site in any previous step influences the landing of a future particle onto the cluster. Therefore, the growth of the cluster in our model is a history-dependent stochastic process.

RESULTS AND DISCUSSION

Figure 2 shows distinct growth scenarios in the morphological evolution of the growing cluster at different values for p_t. A cluster is composed of elementary blue squares. N is the total number of occupied sites as well as the frame number, because one site is occupied in each step. From Figure 2, we clearly see that a highly elongated ribbon structure forms at low p_t. For $p_t = 0.01$ (the upper three figures in Figure 2), in the initial growth stage when the line becomes sufficiently long a lateral site gains an appreciably high probability to be occupied. Quantitatively, the probability that any of the $2n$ lateral sites (n is the length of the line) is occupied is

$$\alpha(n) = 1 - \frac{1}{1 + n\left(\frac{p_t}{p_l}\right)} \tag{3}$$

DOI: 10.1021/acs.jpcb.6b01789
J. Phys. Chem. B 2016, 120, 5960−5965

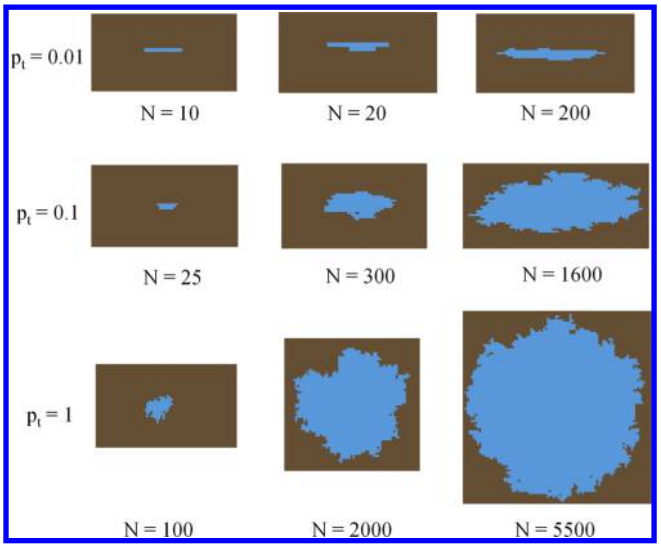

Figure 2. Typical snapshots of the morphologies of occupied sites at different values for p_t. The total number of occupied sites N is the frame number; one site is occupied in each step in the update of the system.

where the second term is the probability that either of the two end sites are occupied. Equation 3 shows that the probability for the appearance of an occupied lateral site increases with the extension of the line, suggesting the instability of a sufficiently long linear cluster toward the transverse propagation. For $p_t = 0.01$ and $p_l = 1$, we have $\alpha(10) = 9\%$, $\alpha(50) = 33\%$, and $\alpha(100) = 50\%$. In the limit of $p_t \to 0$, eq 3 shows that the probability of any transverse growth vanishes as expected. The directional growth to form a linear structure in the condition of $p_t \to 0$, realizable in systems with strong directional bonding, corresponds to the filamentous growth.[25] For larger p_t (or n), the probability of occupying a lateral site is significantly increased: $\alpha(n = 10; p_t = 0.1) = 50\%$, and $\alpha(n = 10; p_t = 1) = 91\%$. For $p_t = 1$, Figure 2 shows the isotropic growth of the cluster; the radial extension of the boundary roughness is suppressed in a larger system by comparing the clusters of 2000 and 5500 occupied sites.

In the growing cluster, we numerically observe the emergence of two types of defects: step defects and vacancies. These defect structures can guide the growth process toward the formation of compact clusters instead of fractal configurations.[18] The occupied lateral sites attached to a growing line create the step defects (see the configuration of $p_t = 0.01$, $N = 20$ in Figure 2). According to the model [see eq 1], the corners at the step defects have relatively high probability to be occupied in the update of the configuration. Consequently, the step defects lead to the scanning-like growth to finish the layer created by the newly occupied lateral sites, where the step defects become the fronts of the longitudinal growth. Such a growing mode is responsible for the suppressed lateral growth at low p_t. With the increase of p_t, the probability of the simultaneous growth of multiple layers increases, which promotes the lateral growth of the cluster. Furthermore, as the consequence of the scanning growth occurring at neighboring layers, vacancies start to appear as shown in the cases of $p_t = 0.1$ and 1.0 in Figure 2. These vacant sites surrounded by three or four occupied neighboring sites have an even higher probability of being occupied than a step defect according to the rule of the model. We numerically observe that these vacancies, once appear, are filled within a few subsequent steps. The removal mechanism of vacancies prevents the formation of fractal configurations.

Simulations show that the roughness in the contour of a growing cluster is greatly reduced by summing over a number of statistically independent configurations. We obtain sufficiently smooth averaged clusters over 20 independent simulation runs as shown in Figure 3; the brighter region is of higher density. Note that averaging over only 10 independent simulation runs can generate sufficiently smooth clusters; increasing the number of simulation runs can lead to even sharper clusters. By averaging out the boundary roughness, all the oval shapes in Figure 3 are found to converge to the elliptic curves

$$\frac{(x - x_0)^2}{a^2} + \frac{(y - y_0)^2}{b^2} = 1 \tag{4}$$

The values for the fitting parameters (a, b) in the configurations in Figure 3 are (120, 13), (170, 18), and (210, 23) for $p_t = 0.01$ and (66, 23), (95, 32), and (115, 40) for $p_t = 0.1$, respectively. As a history-dependent stochastic process in our model, the occupation of a site in any previous step influences the landing of a future particle onto the cluster. Such a convoluted growth process imposes a formidable challenge for explicit analytical analysis of the system.[17] Here, computer simulations reveal that the sum of independent growth processes with long-range temporal correlations can eliminate the uncertainties in the model represented by various rough boundaries and ultimately converge to deterministic elliptic patterns.

Remarkably, we further find that a/b is an invariant in each instantaneous moment in the growth process for given p_t by analyzing the clusters in Figure 3. The invariance of the ratio a/b is also confirmed in systems with other typical values for p_t, and the results are summarized in Figure 4a. Figure 4a shows that all the simulation data at the same p_t uniformly fall on the same fitting line. To conclude, all the averaged growing clusters at the same p_t derived from our model are self-similar; a scaling transformation bridges a cluster at different growing stages. The degree of the ovalness reflects the ratio of the transverse to the longitudinal growth probabilities p_t/p_l as well as the relative strength of the physical interactions along these two directions.

Figure 4b shows the nonlinear dependence of the ratio a/b versus p_t. A striking feature in the a/b–p_t curve is the high steepness occurring at $p_t/p_l \approx 0.1$, which signifies a phase transition-like behavior at this critical value for p_t. The significant deviation of the averaged cluster from a circular shape occurs for $p_t/p_l < 0.1$. It is in the regime of low p_t/p_l that can generate the experimentally observed elongated ribbon structures for the much stronger π–π stacking and the weaker edge–edge stacking in the longitudinal and transverse directions, respectively.[15] It is interesting to note that experimentally, a change from ribbons to sheets occurs as noted in ref 15 when the ionic concentration changes, suggesting that the ratio of p_l to p_t can be modified by the solvent conditions. At this point, our approach cannot be directly compared with this experiment because further systematic studies are required and it is experimentally challenging to tune these molecular interactions. In Figure 4a, for the data points along each line from left to right, N starts from 1000 at the increment of 1000. The denser point distribution approaching the right-hand side of each line indicates the slow-down of the growth. Figure 4c,d shows the growth of the width and length of the cluster along the vertical and horizontal central lines, respectively. We see that for a smaller p_t the cluster grows faster in the longitudinal direction and slower in the transverse direction. Figure 4c,d shows that the slopes of both growth curves are reduced in time,

DOI: 10.1021/acs.jpcb.6b01789
J. Phys. Chem. B 2016, 120, 5960–5965

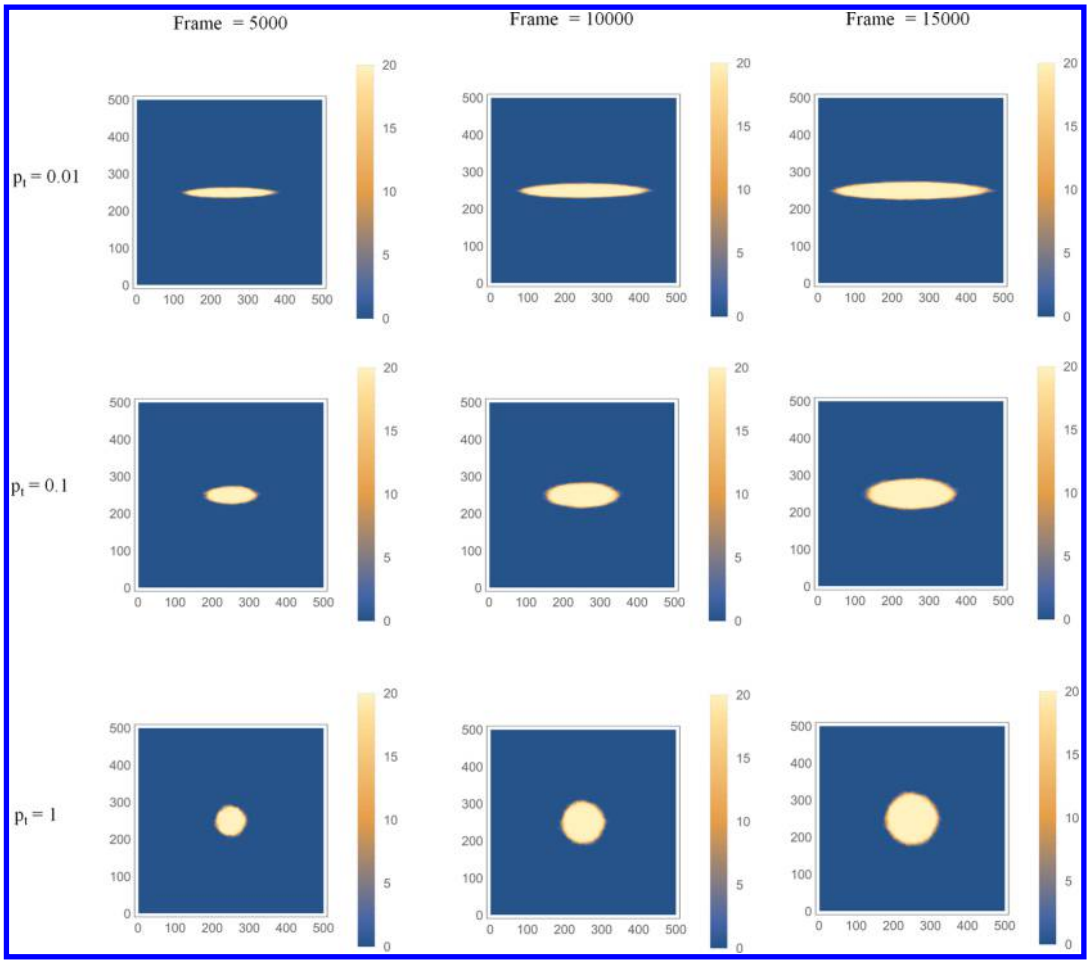

Figure 3. Plot of the averaged configurations (over 20 independent simulation runs) of a growing cluster at different values for p_t. Highly elongated ribbon structures form at low values for p_t through the layer-by-layer scanning-like growth mode.

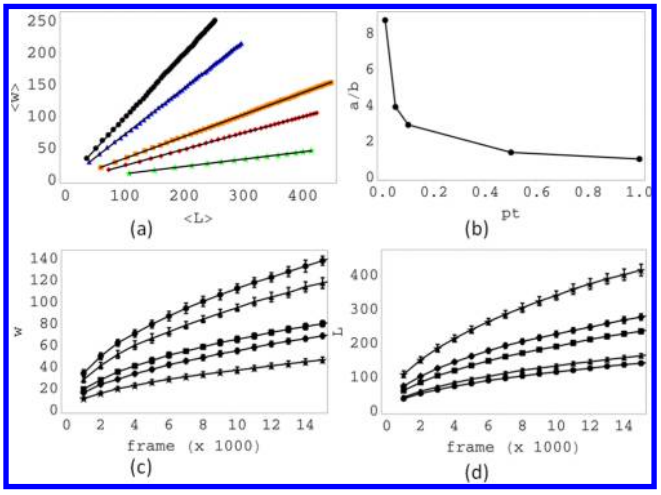

Figure 4. Geometric analysis of the growing cluster. (a) The plot of the averaged ribbon width w versus the averaged length L during its growth over 20 independent simulations runs. The cluster becomes more anisotropic with the reduction of p_t from 1.0 (circle, black), 0.5 (triangle, blue), 0.1 (square, orange), 0.05 (diamond, red), to 0.01 (star, green). The relation of a/b and p_t in (b) is derived from (a). $\langle L \rangle = 2a$. $\langle w \rangle = 2b$. (c,d) The growth of the cluster width and length, respectively. The error bars showing the standard deviation are obtained from 20 independent simulation runs. p_t = 0.01 (star), 0.05 (diamond), 0.1 (square), 0.5 (triangle), and 1.0 (circle). p_l = 1.

suggesting that ultimately the growth process is practically frozen. We further find that all the curves in Figure 4c,d perfectly conform to a uniform power law with the exponent 1/2; the fitting curves in the functional form of $a + bt^{\gamma}$ well coincide with the simulation data by choosing proper values for the fitting parameters a and b.

We proceed to explore the origin of the self-similarity phenomenon revealed in our model. It is speculated that the self-similarity in each instantaneous shape of a growing cluster may require the delicately coordinated growth of different parts in the cluster. However, our calculations show the statistical independence of the growth by analyzing the correlation between the width $w(x_0)$ along the vertical line (at $x = x_0$) and the width $w(x)$ along the line at x.

Figure 5 shows the plot of $C(x) = \langle w(0)w(x) \rangle$ (black curves with larger plot markers) as well as $\langle w(0) \rangle \langle w(x) \rangle$ (red curves with smaller plot markers). The coincidence of these two curves, that is, $\langle w(0)w(x) \rangle = \langle w(0) \rangle \langle w(x) \rangle$ indicates the statistical independence of the growing width over the cluster. The statistical independence also occurs for the cases of x_0 = 10, 20, and 30. The lack of statistical correlation in the growth of the cluster width suggests that the realization of the self-similar patterns does not require the coordinated growth of different parts in the cluster. The establishment of the specific connection between the statistical independence and the self-similar growth process may rely on the presently formidable analytical analysis of the model.[17]

DOI: 10.1021/acs.jpcb.6b01789
J. Phys. Chem. B 2016, 120, 5960−5965

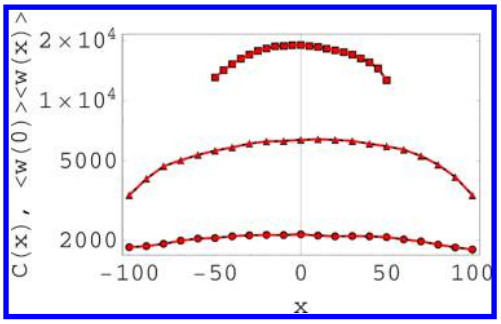

Figure 5. Coincidence of the $C(x) = \langle w(0)\, w(x)\rangle$ curve (black curves with larger plot markers) and the $\langle w(0)\rangle\langle w(x)\rangle$ curve (red curves with smaller plot markers) indicates the statistical independence of the transverse growth in the cluster. $w(x)$ is the width along the vertical line at x; $x = 0$ in the central vertical line passing through the cluster. The average procedure is over 20 independent simulation runs. $N = 15\,000$.

CONCLUSIONS

In summary, we present the anisotropic stochastic growth model to rationalize the experimentally observed self-assembly of the elementary CA molecules to fabricate the coherent ribbon structures.[15] Simulations show the formation of highly elongated ribbon-like clusters by a scanning-like growth mode in the regime of $p_t < 0.1$, where p_t is the ratio of the transverse to the longitudinal growth rate. This model reveals the convergence of rough clusters toward regular elliptic patterns by averaging over a number of independent growth processes. The nonlinear relation between the aspect ratio of the elliptic cluster and the value for p_t is established. Remarkably, the averaged elliptic cluster is self-similar in its growth; the entire growth process can be constructed by a scaling transformation. Further statistical analysis suggests that the realization of the self-similar pattern does not rely on the delicately coordinated growth of different parts in the cluster.

The ordered self-similar patterns revealed in this work have wider implications, notably, in using anisotropic interactions to design both 2D and 3D aggregates with desired exterior shapes. The conclusions derived from this idealized model, especially the connection between the cluster shape and the anisotropic interaction, may also be used to interpret the behaviors of active matters. The effect of the activity in general active colloidal and nematic systems is well characterized by the effective interaction potential or active stress.[26,27] It is therefore speculated that in the recent work the dynamic deformation of the cluster boundary enclosing a collection of active spinners may result from the temporally evolving effective anisotropic interaction between the active colloidal particles.[28]

AUTHOR INFORMATION

Corresponding Author

*E-mail: m-olvera@northwestern.edu.

Notes

The authors declare no competing financial interest.

ACKNOWLEDGMENTS

This work was supported as part of the Center for Bio-Inspired Energy Science, an Energy Frontier Research Center funded by the U.S. Department of Energy, Office of Science, Basic Energy Sciences under Award No. DE-SC0000989-002. Z.Y. acknowledges the support from SJTU startup fund and the award of the Chinese Thousand Talents Program for Distinguished Young Scholars.

REFERENCES

(1) Kamien, R. D. Topology From the Bottom Up. *Science* **2003**, *299*, 1671.
(2) Lash, M.; Fedorchak, M.; McCarthy, J.; Little, S. Scaling Up Self-Assembly: Bottom-Up Approaches To Macroscopic Particle Organization. *Soft Matter* **2015**, *11*, 5597−5609.
(3) DeVries, G. A.; Brunnbauer, M.; Hu, Y.; Jackson, A. M.; Long, B.; Neltner, B. T.; Uzun, O.; Wunsch, B. H.; Stellacci, F. Divalent Metal Nanoparticles. *Science* **2007**, *315*, 358−361.
(4) Wang, Y.; Wang, Y.; Breed, D. R.; Manoharan, V. N.; Feng, L.; Hollingsworth, A. D.; Weck, M.; Pine, D. J. Colloids with Valence and Specific Directional Bonding. *Nature* **2012**, *491*, 51−55.
(5) Ershov, D.; Sprakel, J.; Appel, J.; Cohen Stuart, M. A.; van der Gucht, J. Capillarity-Induced Ordering Of Spherical Colloids on an Interface with Anisotropic Curvature. *Proc. Natl. Acad. Sci. U. S. A.* **2013**, *110*, 9220−9224.
(6) Garmann, R. F.; Sportsman, R.; Beren, C.; Manoharan, V. N.; Knobler, C. M.; Gelbart, W. M. A Simple RNA-DNA Scaffold Templates the Assembly of Monofunctional Virus-Like Particles. *J. Am. Chem. Soc.* **2015**, *137*, 7584−7587.
(7) Walther, A.; Müller, A. H. Janus Particles. *Soft Matter* **2008**, *4*, 663−668.
(8) Wang, Y.; Hollingsworth, A. D.; Yang, S. K.; Patel, S.; Pine, D. J.; Weck, M. Patchy Particle Self-Assembly via Metal Coordination. *J. Am. Chem. Soc.* **2013**, *135*, 14064−14067.
(9) Rupich, S. M.; Talapin, D. V. Colloidal Self-Assembly: Interlocked Octapods. *Nat. Mater.* **2011**, *10*, 815−816.
(10) Sacanna, S.; Irvine, W.; Chaikin, P. M.; Pine, D. J. Lock and Key Colloids. *Nature* **2010**, *464*, 575−578.
(11) Cui, H.; Pashuck, E. T.; Velichko, Y. S.; Weigand, S. J.; Cheetham, A. G.; Newcomb, C. J.; Stupp, S. I. Spontaneous and X-ray-Triggered Crystallization at Long Range in Self-Assembling Filament Networks. *Science* **2010**, *327*, 555−559.
(12) Aida, T.; Meijer, E.; Stupp, S. Functional Supramolecular Polymers. *Science* **2012**, *335*, 813−817.
(13) Safinya, C. R. Structures of Lipid-DNA Complexes: Supramolecular Assembly and Gene Delivery. *Curr. Opin. Struct. Biol.* **2001**, *11*, 440−448.
(14) Hasegawa, M.; Iyoda, M. Conducting Supramolecular Nanofibers and Nanorods. *Chem. Soc. Rev.* **2010**, *39*, 2420−2427.
(15) Weingarten, A. S.; Kazantsev, R. V.; Palmer, L. C.; McClendon, M.; Koltonow, A. R.; Samuel, A. P.; Kiebala, D. J.; Wasielewski, M. R.; Stupp, S. I. Self-Assembling Hydrogel Scaffolds for Photocatalytic Hydrogen Production. *Nat. Chem.* **2014**, *6*, 964−970.
(16) Amunts, A.; Drory, O.; Nelson, N. The Structure of a Plant Photosystem I Supercomplex at 3.4 Å Resolution. *Nature* **2007**, *447*, 58−63.
(17) Neyman, J. *Proceedings of the Fourth Berkeley Symposium on Mathematical Statistics and Probability*; University of California Press: Oakland, CA, 1961.
(18) Witten, T., Jr; Sander, L. M. Diffusion-Limited Aggregation, a Kinetic Critical Phenomenon. *Phys. Rev. Lett.* **1981**, *47*, 1400.
(19) Stanley, H. E.; Ostrowsky, N. *Random Fluctuations and Pattern Growth: Experiments and Models*; Springer Science & Business Media: Oakland, CA, 2012; Vol. *157*.
(20) Wettlaufer, J.; Jackson, M.; Elbaum, M. A Geometric Model for Anisotropic Crystal Growth. *J. Phys. A: Math. Gen.* **1994**, *27*, 5957.
(21) Ivanenko, Y. V.; Lebovka, N.; Vygornitskii, N. Eden Growth Model for Aggregation of Charged Particles. *Eur. Phys. J. B* **1999**, *11*, 469−480.
(22) Smith, R.; Collins, S. Generalized Model for the Diffusion-Limited Aggregation and Eden Models of Cluster Growth. *Phys. Rev. A: At., Mol., Opt. Phys.* **1989**, *39*, 5409.
(23) Wang, C.; Liu, P.; Bassingthwaighte, J. Off-Lattice Eden-C Cluster Growth Model. *J. Phys. A: Math. Gen.* **1995**, *28*, 2141.

DOI: 10.1021/acs.jpcb.6b01789
J. Phys. Chem. B 2016, 120, 5960−5965

(24) Eden, M.; Thevenaz, P. History of a Stochastic Growth Model. *Proc. SPIE* **1997**, 43−54.
(25) Pollard, T. D.; Cooper, J. A. Actin, a Central Player in Cell Shape and Movement. *Science* **2009**, *326*, 1208−1212.
(26) Marchetti, M.; Joanny, J.; Ramaswamy, S.; Liverpool, T.; Prost, J.; Rao, M.; Simha, R. A. Hydrodynamics of Soft Active Matter. *Rev. Mod. Phys.* **2013**, *85*, 1143.
(27) Farage, T.; Krinninger, P.; Brader, J. Effective Interactions in Active Brownian Suspensions. *Phys. Rev. E* **2015**, *91*, 042310.
(28) Spellings, M.; Engel, M.; Klotsa, D.; Sabrina, S.; Drews, A. M.; Nguyen, N. H.; Bishop, K. J.; Glotzer, S. C. Shape Control and Compartmentalization in Active Colloidal Cells. *Proc. Natl. Acad. Sci. U. S. A.* **2015**, *112*, E4642−E4650.

DOI: 10.1021/acs.jpcb.6b01789
J. Phys. Chem. B 2016, 120, 5960−5965